Assessment of Structure-borne Sound Intensity of Solid Wood Walls using a Scanning Laser Doppler-Vibrometer

Schoenwald, Stefan
Tröbs, Hans-Martin
Laboratory for Acoustics/Noise Control, Empa Swiss Federal Laboratories for Materials Science and Technology, Überlandstrasse 129, 8600 Dübendorf, Switzerland.

Summary
The assessment of structure-borne sound intensity is a very useful tool to visualize the power flow due to flexural waves in plates, beams and shells. In this research the structure-borne sound intensity is determined from the surface velocity distribution of a vibrating structure using a well-established finite differences approach. Velocity data measured in a dense grid on the surface of an orthotropic solid wood wall with a scanning laser Doppler vibrometer was used to calculate the structural power flow. As further input data the flexural wavenumbers along the different principal directions of an orthotropic solid wood wall were required and thus were measured as well. The wall was part of a building junction that supported a segmented prefabricated concrete-wood composite floor, so that it was possible to excite the wall directly or indirectly across the building junction. The power flow in the wall was visualized for different excitation cases, for example by a single point force on the wall or on one floor segment, as well as by a distributed excitation of the complete floor with airborne sound. Besides qualitative also energetic considerations on the power flow are made for the validation of the applied methods.

PACS no. 43.40.Le, 43.55.Rg

1. Introduction

The assessment and mapping of structural intensity is a very useful tool to visualize and understand the power flow caused by propagating flexural waves in plate and shell like structures. Once important components for structure-borne sound transmission namely the sources, sinks and transmission mechanisms between coupled elements, are identified in buildings that determine the so-called flanking sound transmission, measures for noise control can be planned efficiently. Unfortunately, structures in lightweight and wooden construction often are not homogenous and usually consist of many elements, such as plates and beams that are connected mechanically with screws and nails. Therefore usually no detailed computational model of the structure exists, from which the required forces, moments and displacements within the structure can be obtained directly to compute the structure-borne sound intensity. Nevertheless, different approaches exist to determine the structure-borne sound intensity in plates from either the calculated or measured out-of-plane surface displacement of vibrating plates and shells. All of these methods assume homogenous plates and most use the finite difference approach to evaluate the spatial derivatives from out-of-plane velocity. The first methods were further restricted to thin isotropic plates and assumed a free propagating wave in the far field, which significantly reduced the instrumentational effort [1,2]. Later, a more sophisticated method was proposed [3] that is also valid for the nearfield for example close to sources, boundaries or discontinuities. However, the simultaneous measurement of the surface velocity at a minimum of 8 positions was required, which was experimentally not feasible at this time. Besides the finite difference approach other approaches, such as spatial Fourier Transform methods [4,5] to determine the spatial derivatives or trial functions to describe the vibrational field [6] were applied to calculate the structure-borne sound intensity in plates. Besides this fundamental work, the methods were already applied on building structures for power flow investigations e.g.

[7,8,9]. However, main focus was on thin isotropic homogenous plates and only limited research exists on orthotropic plates [10,11]. In the following a validation study is presented where these two methods were applied to map the structure-borne sound intensity in solid wood walls, so-called Cross Laminated Timber (CLT) panels. CLT is an emerging wood material that consists of an odd number of layers of cross wise glued wooden beams and therefore exhibits orthotropic properties. In this study the plate velocity was measured in a grid on the plate surface using a scanning laser Doppler vibrometer.

2. Structure-borne Sound Intensity

The applied intensity methods are all for homogenous thin plates. Although CLT is a layered material with limited shear stiffness, this behavior is taken into account by homogenization of the plates by using frequency dependent input data for the stiffness.

2.1. General Formulation

The structural intensity component I_x in x-direction of a plate is given as the sum of its three components that are linked to shear force I_{xS}, bending moment I_{xM} and twisting moment I_{xT}.

$$I_{xS} = \frac{\partial}{\partial x}\left(D_x \frac{\partial^2 w}{\partial x^2} + H \frac{\partial^2 w}{\partial y^2}\right)\left(\frac{\partial w}{\partial t}\right) \quad (1)$$

$$I_{xM} = -D_x \left(\frac{\partial^2 w}{\partial x^2} + \nu_y \frac{\partial^2 w}{\partial y^2}\right)\left(\frac{\partial^2 w}{\partial x \partial t}\right) \quad (2)$$

$$I_{xT} = -2D_{xy} \left(\frac{\partial^2 w}{\partial x \partial y}\right)\left(\frac{\partial^2 w}{\partial y \partial t}\right) \quad (3)$$

All components can be expressed as a function of the spatial ($\partial x, \partial y$) and time derivatives (∂t) of the out-of-plane surface displacement w. They further depend on the bending stiffness D_x in x-direction, the effective torsional stiffness 2H, the torsional stiffness D_{xy} and the Poisson's ratio ν_y.

2.2. Orthotropic Plates

For an orthotropic plate aligned with its x- and y direction along the principal axis of its orthotropy, D_x is given by Equation 4 as function of the plate thickness h, the Youngs'-modulus E_x and the Poisson's ratios ν_x and ν_y. D_y is determined analogously simply by substituting x and y. The effective torsional rigidity H is given by equation 5.

$$D_x = \frac{h^3 \overline{E_{xx}}}{12} = \frac{h^3 E_x}{12\,(1-\nu_x \nu_y)} \quad (4)$$

$$H = \nu_x D_y + 2D_{xy} \quad (5)$$

For a naturally orthotropic plate the direction of bending wave propagation and power flow are only equal for the x- and y-direction. For all other angles of wave propagation θ theoretically the direction of wave propagation and energy flow are different due to the stresses normal to the wave direction [12].

2.3. Applied Methods

In the study three different methods, all use the finite difference approach, were applied to determine the structure-borne sound intensity from the out-of-plane velocity that was measured with a scanning laser Doppler vibrometer in an evenly spaced grid with spacing Δ between neighboring points in the x- and y-direction that are aligned with the principal axis of orthotropy. Since the velocities are not measured simultaneously the so-called frequency-response technique is applied to determine the phase relationship between the measured signals [13].

2.3.1. Method Noiseux

The first method is the simplest intensity approach [1]. A far field away from discontinuities on the plate is assumed, where the force component and the sum of moment components are equal, and hence only the first needs to be evaluated. Further, it is developed for isotropic plates and the difference in the direction of wave and energy propagation is neglected. An array of four points is necessary as shown in Figure 1 to determine the x-component of intensity according to Equation 6 and analogously for the y direction.

$$I_{x,Nois} = -\frac{2\sqrt{D_x m''}}{\Delta} Im\{G_{12}\} \quad (6)$$

Im{} denotes the imaginary part of the cross-spectrum G_{12} of the velocities at point 1 and 2 and m" is the mass per unit area of the wall. When the intensity component in y-direction is determined the stiffness for this particular axis is used.

2.3.2. Method Simon

The method described by Simon [10] is also a so-called far field method. However, first it estimates the approximate angle θ of wave propagation from the two cross-spectra G_{12} and G_{34} in Figure 1 using Equation 7. Then the bending wavenumber $k_{app}(\theta)$ for this approximate direction is determined and the difference in wave and energy propagation direction is taken into account in Equation 8 for the x-component, when the intensity is calculated.

$$tan\,\theta_{app} = \frac{Im\{G_{34}\}}{Im\{G_{12}\}} \quad (7)$$

$$I_{x,Sim} = -\frac{h^3 k_{app}^2(\theta)}{\Delta\omega}\left(\overline{E_{xx}} + \left((\nu_{x-1})\overline{E_{xx}} + 2D_{xy}\right) sin^2\left(\theta_{app}\right)\right) Im\{G_{12}\} \quad (8)$$

Simon claims that for plates with a small difference in stiffness along the principal direction the results of his method agree well with ones of the Method Noiseux.

2.3.3. Method Mandal

The third method explicitly evaluates all components in Equation 1 to 3 and by that takes into account the particularities of thin orthotropic plates. However, for only one direction the velocity has to be known at 7 points located as shown in Figure 1 and 15 different cross-spectra have to be evaluated. The intensity in x-direction is given in Equation 9.

$$\begin{aligned} I_{x,Man} = -\frac{1}{2\omega\Delta^3}\big[Im\{&\left(8D_x + 4D_x\nu_y + 4H\right)G_{36} - 2D_xG_{38} + 2D_xG_{61} + \\ &\left(H - D_x\nu_y\right)G_{32} + \left(H - D_x\nu_y\right)G_{34} - \\ &\left(H + D_x\nu_y\right)G_{35} - \left(H + D_x\nu_y\right)G_{37} + \\ &\left(H + D_x\nu_y\right)G_{62} + \left(H + D_x\nu_y\right)G_{64} - \\ &\left(H + D_x\nu_y\right)G_{65} - \left(H - D_x\nu_y\right)G_{67} + \\ &D_{xy}(G_{25} - G_{27} - G_{45} + G_{47})\}\big] \end{aligned} \quad (9)$$

Again analogously to Equation 9 the intensity component in y-direction has to be determined so that in total 30 cross-spectra have to be known.

2.4. Input data for Materials

The determination of the flexural wave speed as well as its values for a 80 mm CLT plate used in this study are given in the two principal directions in [14]. The direction dependent bending wavenumber can be determined from the bending stiffness in the direction according to Equation 10.

$$D(\theta) = D_x cos^4\theta + 2H cos^2\theta sin^2\theta + D_y sin^4\theta \quad (10)$$

$$H = \nu_x D_y + 2G_{xy}\frac{h^3}{12} \approx \sqrt{D_x D_y} \quad (11)$$

The effective torsional stiffness H is a function of the in-plane shear stiffness D_{xy} and the shear modulus G_{xy} as shown in Equation 11. Since G_{xy} cannot be easily determined experimentally, a well-established approximation according to [15] is used. Further, it is assumed $\sqrt{\nu_x \nu_y} \approx 0.3$.
The bending wavenumbers for the 80 mm CLT are presented in Figure 2 from 50 Hz to 800 Hz, which is the relevant frequency range in this study. There it exhibits only a relatively weak orthotropy.

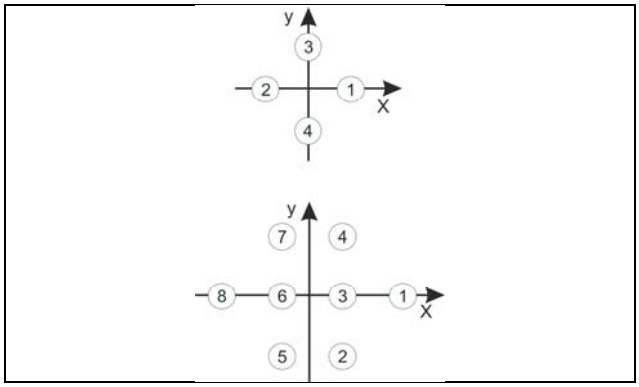

Figure 1. Arrays of measurement points for determination of intensity vector for Method Noiseux and Simon (top) and for Method Mandal only x-component (bottom).

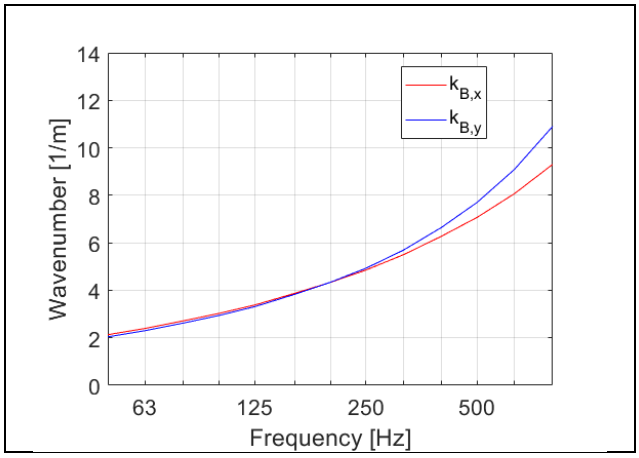

Figure 2. Bending wavenumbers for the two principal directions of the 80 mm CLT wall from 50 Hz - 800 Hz.

3. Experimental Set-Up

The experimental set-up and test specimen is the same as already described in [16] for the calculation of the radiated sound power from the surface velocity.

3.1. Empa Flanking Facility

The Flanking Facility for lightweight construction on the Empa-Campus in Dübendorf was realized and is operated with the Berne University of Applied Sciences in Biel. The facility can accommodate test specimens that divide the space into a maximum of four rooms, with two on the ground floor and two above. One side and one back wall of the facility consist of a permanent concrete L-shaped structure, the so-called backbone, to provide the necessary structural support for the specimens. After installation of a specimen missing walls and floors are added with

movable wooden wall and roof elements that belong to the facility. This gives a very flexible system suitable for all kind of investigations. Further, all facility walls and floors have a very high direct and flanking sound insulation to avoid sound transmission between rooms and from the outside.

Figure 3 shows a three-dimensional sketch of the facility with the set-up with two rooms one-above-the-other separated by a T-junction that is considered in this paper. The brown elements are the test specimen, grey indicates the permanent structure and in red the movable walls and floors of the facility.

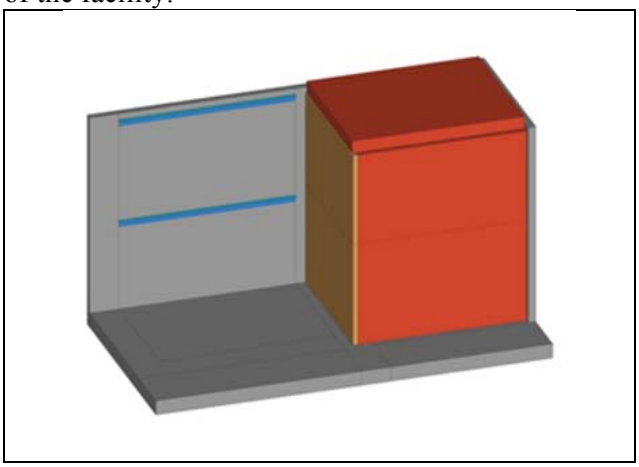

Figure 3. Sketch of the Empa Flanking Facility with the two room set-up considered in this paper (grey: permanent strucutrue of facilty, red: movable facility walls and floors, brown: T-junction under test).

3.2. Test specimen

The test specimen was a T-junction made of a wood-concrete composite floor (HBVR) with a 80 mm thick cross laminated solid wood wall (CLT, mass-per-area: 38 kg/m^2) below and on top. The floor consisted of a 70 mm thick reinforced concrete slab on a 12 mm wooden subfloor that rested on 260 mm high and 80 mm wide wooden joists spaced 440 mm on center. Both, slab and joists were shear connected. The cavity between the joists was filled with 120 mm thick glass fiber batts. Elastic connectors (17 mm high) were attached to the underside of the joists and supported a 24 mm wood furring with a single layer directly attached 12.5 mm thick gypsum board ceiling.

The floor size was 4.50 m by 5.50 m with the wood joists oriented along the long axis. The concrete slab rested on top of the lower CLT wall and the joists that are perpendicular to the junction were connected with angle brackets to it. The upper CLT wall rested on the concrete and was secured with only two angle brackets over the whole length. In the middle along the joists the floor was split into two equally wide prefabricated elements. Their rebar was welded together at two spots and the small gap in the slab between the two floor elements was filled with grout. The number of connections between the specimen and the facility were minimized, elastically supported and sealed to prevent sound leaks.

3.3. Test Set-up

The velocity of the lower wall of the specimen was measured with a scanning laser Doppler vibrometer from the outside of the facility in a grid with 26 rows by 43 columns with points evenly spaced approximately 0.10 m. The specimen was excited from the inside with an electrodynamic shaker that was driven by pseudo-random noise. The shaker was attached with stinger using an impedance head. Two excitation positions are presented in this study. The first is somewhat of the center of the lower wall. The second is on the floor in the upper room on the left of the two prefabricated floor slabs. In this case the wall is excited only indirectly at its upper edge across the building junction.

The force signal of the impedance was used as phase-reference for the velocity measurement and its acceleration signal was used to determine the injected power from the cross-spectrum of the force and acceleration at the excitation point. The time signals were transformed into the frequency domain. From the FFT-spectra with 3200 lines from 0 Hz to 6400 Hz the intensity is calculated, and in a second step band filtered to obtain one-third octave bands to reduce the amount of information. The same processing was conducted with the injected power. The spectra were further low-pass filtered to remove intensity components where for the point spacing in either one direction the condition $\Delta \leq 0.4\lambda_{Bx,y}$ was not fulfilled to avoid aliasing.

4. Results

In the following the results are presented for both excitation positions, one directly on the wall and one on the left floor slab in the room above.

4.1. Excitation of wall with shaker

In this case the wall was directly excited with shaker at a position somewhat left from the center of the wall. First, exemplarily vector maps are shown for all three methods. Since the power injected in the wall can be determined in this case directly from the cross-spectrum of the signals of the impedance head, also the absolute values of intensity were verified by integrating the normal intensity along closed line around the source and the edges of the wall.

4.1.1. Intensity maps and power flow plots

The vector maps as well as so-called streamline plots that depict the power flow from sources to sinks are presented in Figure 6 for all three methods that were applied in this study. The results are all shown for the 200 Hz band. From the plots in the first two rows determined according to the Method Noiseux and Simon it is obvious that both are almost identical. The source can be clearly identified at position (0m,0m) and most power flows from the source away to the left

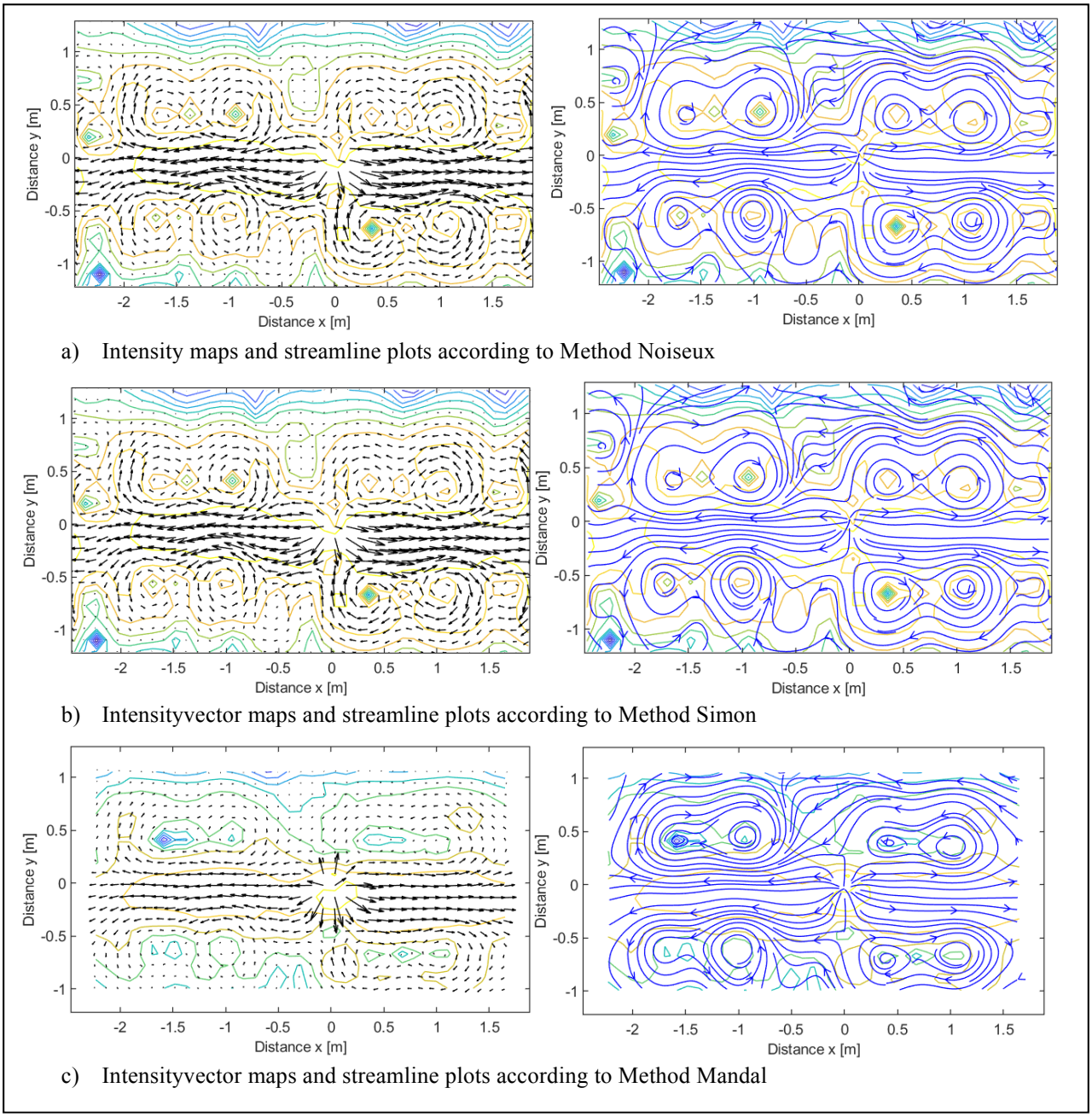

Figure 4. Intensity vector maps and streamline plots of wall with shaker excitation at position at x = 0m and y = 0m at 200 Hz for the three methods.

and right of the source. Further the power circulates around for locations above and below this main flow. These are artefacts caused by standing waves on the plate that do not transport

energy. All applied methods are based on the finite difference approach, which assumes that all displacement is linked to propagating waves that carry energy and therefore displacement due to plate modes are indicated by these vortices. The results for the Method Mandal, which explicitly assumes all forces and moments, are presented in the last row. The size of the vector field is slightly limited around the edges in comparison to the first graph due to the size of the array required to resolve all spatial derivatives. Qualitatively, the results are very similar to the first two methods, however, intensity amplitudes, which will be investigated later, and direction are slightly different. Nevertheless, for identification of sources and sinks all three methods seem to be equally appropriate.

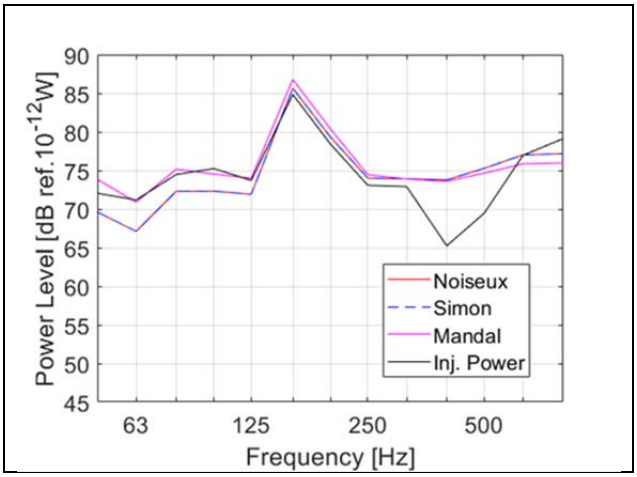

Figure 5. Comparison of injected power at shaker and integration of intensity of different methods along square line with 0.5 m distance to source.

4.1.2. Integration of intensity around source

Next the normal intensity components were integrated along a closed square line with the source in the middle. The minimum distance of the square to the source was 0.5 m on each side as well as on top and bottom. The distance was chosen to avoid mistakes by the two far-field methods due to the nearfield around the source.

The power levels are presented in Figure 5 from 50 Hz to 800 Hz one-third octave bands. The upper limit of 800 Hz was due to the spacing of the measurement points in the grid. Above 800 Hz it is expected that aliasing occurs as the spacing is equal or greater than half a bending wavelength in the wall. The black line is the injected power from the source that was determined from the impedance head signals and chosen as reference.

For its calculation no input data of the wall properties is necessary. The red solid line and the dashed blue are the power levels for the two far-field methods according to Noiseux and Simon.

At 400 Hz and 500 Hz all methods overestimate the power relative to the injected power by a maximum of up to 7 dB, whereas on the other hand the agreement between all methods is very good. The error is likely due to an error in the acceleration signal of the impedance head used. It turned out after the measurement that it is only suitable for the measurement at low and mid frequencies for heavy structures. The casing of the impedance head might resonate depending on the mass of the structure, which affects the measured accelerations signal.

In Figure 6 the power levels from the intensity integrated along all sides of the square around the source are presented as well as the injected power. If the intensity is affected by the orthotropic behavior, it differences could be observed between the methods above 315 Hz depending on the direction of the intensity component. However, above 125 Hz all integrated power levels match very well, so that the influence can be excluded.

4.1.3. Integration along wall boundaries

In Figure 7 the power levels are shown that were determined from the integrated power flow normal to the plate edges for the Method Mandal. The total power level is now slightly lower than the injected power, because besides transmission at the edges also structure-borne sound is attenuated within the plate and radiated as airborne sound. At 400 Hz the injected power level is still higher than the actual power lost along the edges.

Above 250 Hz most power is transmitted at the top and bottom edge, where the wall is connected to surrounding building elements. Below most losses occur at the left and right wall edge, although there the wall is not connected to other elements. Instead a gap filled with elastic porous material exists that does not restrain the wall at its first modes. At these free-edges the out-of-plane displacement is largest and likely vibrational power is therefore efficiently damped due to the deformation of the material in the gap.

4.2. Excitation of left floor element with shaker

Next the left of the two prefab elements of the floor, which is supported at the top of the wall, is excited with the shaker. The wall is excited in this case by the structure-borne sound that is transmitted along the junction at the top of the wall.

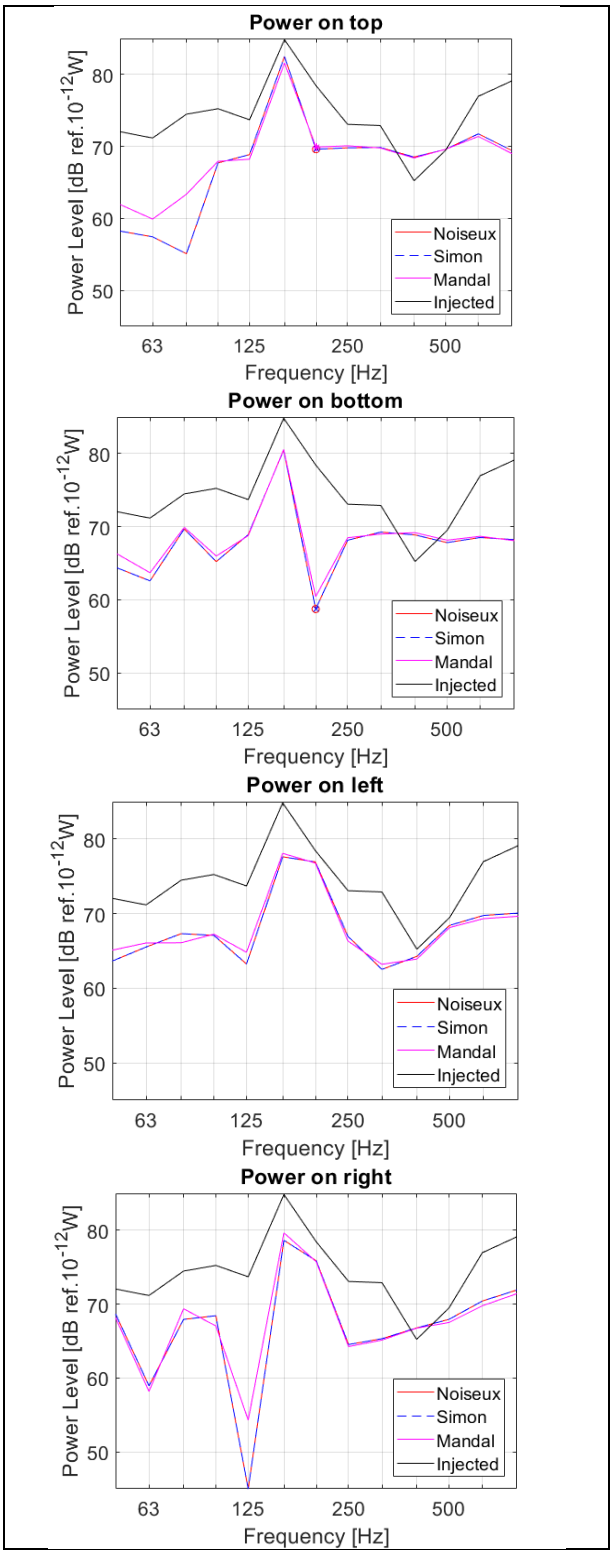

Figure 6. Comparison of injected power at shaker and integration of intensity along line on top, bottom, left and right side of closed square around source. Markers indicate powerflow towards source.

4.2.1. Intensity maps and power flow plots

The intensity vector maps and power flow plots are presented in Figure 9 for the 200 Hz band for the Method Mandal. As expected most power flow occurs at the top left edge towards the wall, transmitted power is much smaller at the top right.

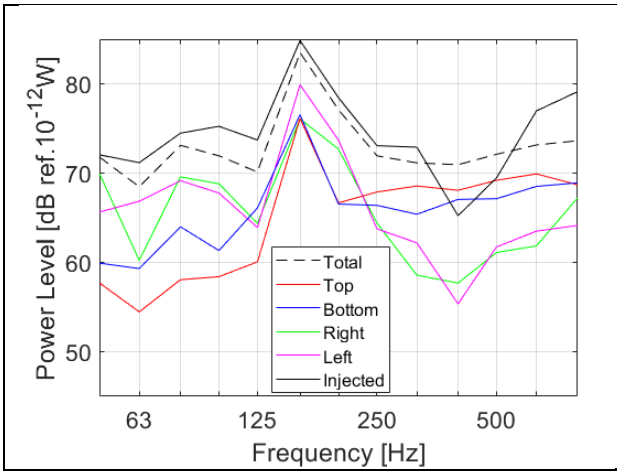

Figure 7. Integration of intensity according to Mandal around plate edges

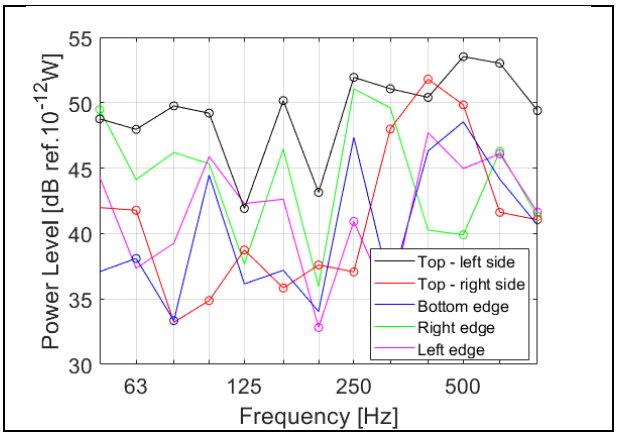

Figure 8. Integration of intensity according to Mandal around plate edges (excitation of floor). Markers indicate powerflow towards the wall.

4.2.2. Integration along wall boundaries

Again the intensity components normal to the edges are integrated along lines. The power levels are presented in Figure 8. Hereby, based on the intensity plots, the upper boundary is split in the middle to compare the power that is transmitted from the left (excited) floor slab (black line) and the right floor slab (red line) that is only weakly connected to the left. The markers indicate power flow towards the wall, data points without markers are power losses.

Most power is indeed transmitted from the left floor slab. Levels are more than 10 dB higher than from the right part except at 400 Hz where both levels are equal. Power transmission from the left floor slab via the right slab to the wall can therefore be almost neglected. At all other edges power is lost.

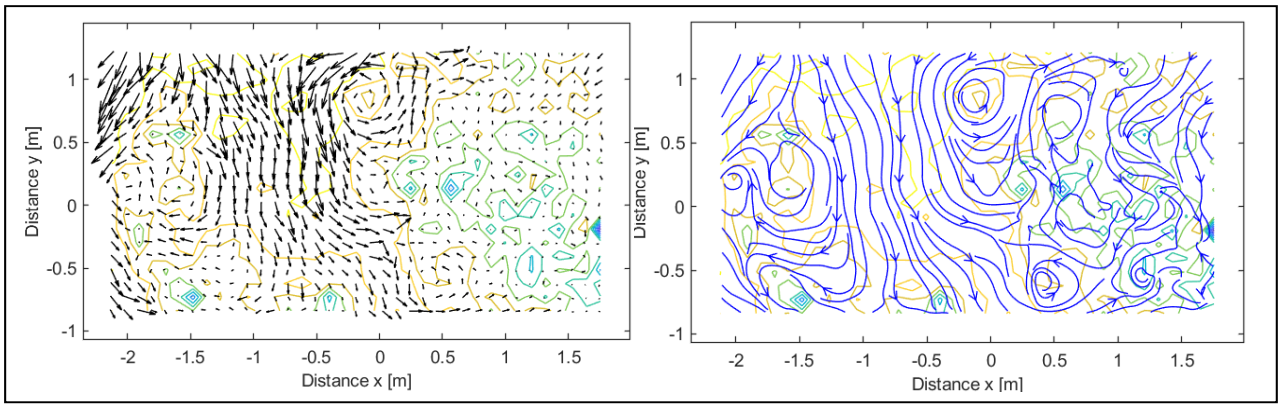

Figure 9. Intensity vector maps and streamline plots of wall with shaker excitation of left floor element at 200 Hz for the Method Mandal.

5. Conclusions

Three different methods to determine the structure-borne sound intensity from measured surface velocity data were applied at a CLT wall. Since the CLT wall had almost isotropic properties in the considered frequency range all methods delivered essentially the same results and are suitable for the identification of sources, sinks and transmission paths. Further, also the absolute value of the intensity was validated by integration along closed paths around the sources and plate edges.

Noiseux's simple method is the easiest to apply since many simplifying assumptions are made. Simon's method takes into account the particularities of orthotropic plates, but for the present case results almost identical to Noiseux. Mandal's method is most sophisticated as it takes into account near field effects as well as the orthotropy. However, the results were found only slightly better at low frequencies, where nearfield have a big influence. The apparent bending wavenumber along the principal axis can be determined. But assumptions were made for the in-plane shear modulus, since it cannot be measured easily. This might have a bigger impact for plates with a higher degree of orthotropy. Therefore a method for its determination would be desirable.

Nevertheless, all applied methods delivered satisfying results for further studies of CLT.

References

[1] D.U. Noiseux,"Measurement of power flow in uniform beams and plates", J. Acoust. Soc., 47(1), 1970

[2] G. Pavic, «Measurement of structure borne wave intensity, Part 1: Formulation of the the methods» J. Sound Vib.,49(2) 1976

[3] M.C.McGary, «Simulated Measurement of powerflow in structures near to simple sources and boundaries», NASA Technical Memorandum #89124, 1988

[4] E.G. Williams, H.D. Dardy, R.G. Fink, «Techniqies for measurement on structure borne intensity in plates», J. Acoust. Soc. AM. 78(6), 1985

[5] J.-C. Pascal, T.Loyau, X. Carniel «Complete determination of structural intensity in plates using Laser Vibrometers», J. Sound Vib., 161(3), 1993

[6] N.B. Roozen, J.L. Guyader, C. Glorieux, "Measurement-based determination of the irrotational part of the structural intensity by means of test functional series expansion", J. Sound Vib., 356, 2015

[7] J.M. Cuschieri, «Experimental measurement of structural intensity on an aircraft Fuselage» Noise Control Eng. 37(3), 1991

[8] S. Schoenwald, B. Zeitler, T.R.T. Nightingale, „Investigation of flanking sound transmission in lightweight building structures using a scanning laser vibrometer",Acoustics Bulletin 35(4), 2010

[9] F. Schöpfer, C. Hopkins, A.R. Mayr, U. Schanda, „Modelling strucutre-borne sound transmission across a timber-frame wall using SEA", Proc. of INTERNOISE 2016, Hamburg, Germany, 2016

[10] F. Simon, S. Pauzin "Strucutral Intensity Formulation and Measurements Validation in the Case of Composite Multi-Layered Panels", Acta Acustica u. w. Acustica, Vol. 92, 2006

[11] N.K. Mandal, R. A. Rahman, M.S. Leong „Strucutre-borne Power Transmission in Thin Naturally Orthotropic Plates: General Case", Journal of Vibration and Control, 9, 2003

[12] I. Bosmans, P. Mees, G. Vermeir "Structure-borne sound transmission between thin orthotropic plates: analytical solutions", J. Sound Vib.,191, 1996

[13] J. Linjama, T. Lahti, "Estimation of the bending wave intensity in beams using the frequency-response technique", J. Sound Vib., 153(1) 1992

[14] A. Santoni, S. Schoenwald, B. Van Damme, P. Fausti "Determination of the elastic and stiffness characteristics of cross-laminated timber plates from flexural wave velocity measurements", J. Sound Vib. Vol. 400, 2017

[15] M.S. Troitsky, "Stiffened Plates: Bending, Stability and Vibration" Elsevier Scientific, Amsterdam

[16] S. Schoenwald, H.-M. Tröbs, A. Zemp, „Measurement of flanking sound transmission at low frequencies with a laser doppler vibrometer", Proc. of EURONOISE 2015, Maastricht, The Netherlands, 2015